
Superconductivity in Li₆P electride

Ziyuan Zhao¹, Shoutao Zhang¹, Tong Yu¹, Haiyang Xu¹, Aitor Bergara^{*,2,3,4} and Guochun Yang^{*,1}

Electrides are unique compounds where most of the electrons reside at interstitial regions of the crystal behaving as anions, which strongly determines its physical properties. Interestingly, the magnitude and distribution of interstitial electrons can be effectively modified either by modulating its chemical composition or external conditions (e.g. pressure). Most of the electrides under high pressure are non-metallic, and superconducting electrides are very rare. In this work we report that a pressure-induced stable Li₆P electride becomes superconductor with a T_c of 39.3 K, which is the highest among already known electrides. The interstitial electrons in Li₆P, with dumbbell-like connected electride states, play a dominant role in the superconducting transition. Other Li-rich phosphides, Li₅P and Li₈P, are also predicted to be superconducting electrides, but with a lower T_c . Superconductivity in all these compounds can be attributed to a combination of a weak electronegativity of P with a strong electropositivity of Li, and opens up the interest to explore high-temperature superconductivity in similar binary compounds.

¹Centre for Advanced Optoelectronic Functional Materials Research and Laboratory for UV Light-Emitting Materials and Technology of Ministry of Education, Northeast Normal University, Changchun 130024, China. ²Departamento de Física de la Materia Condensada, Universidad del País Vasco-Euskal Herriko Unibertsitatea, UPV/EHU, 48080 Bilbao, Spain. ³Donostia International Physics Center (DIPC), 20018 Donostia, Spain. ⁴Centro de Física de Materiales CFM, Centro Mixto CSIC-UPV/EHU, 20018 Donostia, Spain. Correspondence and requests for materials should be addressed to a.bergara@ehu.eus; yanggc468@nenu.edu.cn.

Introduction

Electrides represent a class of extraordinary compounds where some electrons in the solid are localized at interstitial regions, rather than being attached to atoms, and behave as anions[1,2]. The existence of quantized orbitals at the interstitials allows the transfer of electrons there[3]. Although the energies of both interstitial and atomic orbitals increase with pressure, the change of the interstitial orbital energy is usually smaller[4,5]. Thus, formation of electrides can become energetically favorable under high pressure, and various electrides have been already induced by pressure both in elements[6-9] and compounds[10-12]. These interstitial electrons largely determine the physical properties of the electrides[13-15].

Searching for high-temperature superconductivity remains one of the most important topics in condensed matter physics. Even though cuprates[16,17] and Fe-pnictides[18,19], among others, took a leading role on

this pursuit, it is well known that pressure enhances the superconducting properties[20], and hydrogen sulfides[21] and lanthanum hydrides[22] have been recently observed to superconduct with T_c s above 200 K.

On the other hand, even though electrides are usually insulators, recent experiments showed that a canonical electride [Ca₂₄Al₂₈O₆₄]⁴⁺(e⁻)₄ becomes a superconductor ($T_c \sim 0.4$ K)[23-26]. The interstitial electrons in Ca₂₄Al₂₈O₆₄ accommodate loosely in the cages of unit structures, rising an uncommon conductivity. Additionally, Mn₅Si₃-type Nb₅Ir₃[15] and two-dimension Y₂C[27] have been also found to hold both electride states and superconductivity. Additionally, as stated above, it is well known that pressure induces the formation of electrides. For example, both alkaline and alkaline-earth metals form electrides under pressure, as *s* orbital electrons can easily go to interstitial sites[4]. The strong localization of both interstitial and orbital electrons, caused by orbital coupling, makes them

insulating[8,28-31]. However, under higher pressure Li shows a phase transition to a metallic phase while keeping the electrider state (*Cmca*-24 Li at 90 GPa)[32]. Although this is a poor metal, the inclusion of extra elements might adjust interstitial electrons and help to improve its metallic character. For instance, as it was observed in suboxide Li_6O [33] and Ca_2N -type Li_4N [13] electrides, filling free spaces of Li with guest *p*-block elements modifies the electronic band topology and even increases its superconducting T_c [15]. Having this in mind, and considering that P has a moderate electronegativity and it is a remarkable superconductor[34,35], Li phosphides have reasonable expectances to become superconducting electrides. Interestingly, in a recent work a Li_5P metallic electride has been found to be stable under pressure[36]. Li atoms in Li_5P donate the excess electrons into the lattice spaces, forming an unusual 2D electride, with convenient conducting electronic channels.

These distinguishing electronic properties have attracted our attention of Li-P compounds. Herein, compounds with Li_xP stoichiometry have been searched from 50 to 300 GPa, and several superconducting electrides (*i.e.* *C2/c* Li_5P , *P-1* Li_6P , *C2/c* Li_6P and *C2/c* Li_8P) have been found under pressure. In these electrides, electrons gather not only at interstitial sites but also around P atoms. Notably, the superconducting properties of the electrides are determined by their structural configurations (Li_5P , Li_6P and Li_8P). *C2/c* Li_6P , with more connected interstitial electrons, shows the highest T_c value of 39.3 K, which becomes the highest predicted T_c between already reported electrides.

Results and Discussion

Ab initio structure prediction

Various Li-rich phosphides (Li_xP , $x = 1 - 8$) have been searched extensively. Herein, structure prediction calculations were performed at 0 K and selected pressures of 50, 100, 200 and 300 GPa. The formation enthalpy (ΔH), relative to the elemental solids (Li and P), was calculated at each considered pressure according to the equation below:

$$\Delta H(\text{Li}_x\text{P}) = [H(\text{Li}_x\text{P}) - xH(\text{Li}) - H(\text{P})]/(x + 1), \quad (1)$$

where $H = U + PV$ is the enthalpy of each composition, and ΔH is the formation enthalpy per atom of the given compound. Here, U , P , and V are the internal energy, pressure, and volume, respectively. The relative thermodynamic stability of Li_xP stoichiometries at 100, 200

and 300 GPa is shown in Figure 1a, and that at 50 GPa is in Figure S1. Stable phases lie on the global stability line of the convex hull, whereas compounds lying on the dotted lines are metastable with respect to decomposition into other Li_xP compounds or elemental Li and P solids. In addition to the stable LiP (from 63 GPa up to 300 GPa), other Li-rich stoichiometries (Li_3P , Li_5P , Li_6P and Li_8P) are predicted to be stable under increased pressure. The most stable *Fm-3m* Li_3P lies on the convex hulls at the whole pressure range. Additionally, *P6/mmm* Li_5P starts to be stable at 10.3 GPa, and remains stable until 163 GPa. There are two other Li_5P stable phases with increasing pressure: *C2/c* Li_5P is stable between 163 and 249 GPa, while *Cmcm* Li_5P stabilizes above 249 GPa. For the stoichiometries with a higher Li content, Li_6P and Li_8P become stable over 178 GPa and 150 GPa, respectively. *P-1* Li_6P transfers to *C2/c* Li_6P above 271 GPa. The pressure-composition phase diagram is shown in Figure 1b. All the phases in Figure 1b are dynamically stable, as they do not show any imaginary frequency modes (Figure S2).

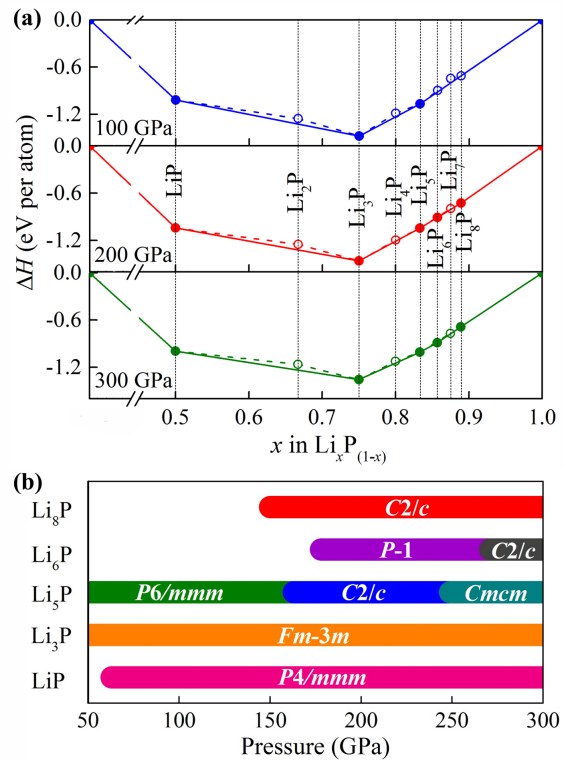


Figure 1. Relative thermodynamic stability of Li_xP at 0 K and different pressures (100, 200 and 300 GPa). (a) The calculated formation enthalpy per atom of Li_xP compounds with respect to elemental Li and P solids. The thermodynamically stable compounds are shown by solid symbols, connected by the solid lines line (convex hull). (b)

Geometry structures of stable Li_xP phases

Pressure-induced LiP compound stabilizes into a tetragonal structure (space group $P4/mmm$, 1 formula unit, Figure 2a), in which each P atom has 8-fold coordination, with Li atoms forming a P-Li cuboid. As Li content increases, the coordination environment of the P atom changes and it becomes hypercoordinated. 15-fold and 17-fold coordinations of P atoms are observed in $C2/c$ Li_5P and $Cmcm$ Li_5P (Figure 2b and 2c), respectively; in $P-1$ Li_6P (Figure 2d) and $C2/c$ Li_8P P atoms show a 16-fold coordination (Figure 2f). Notably, the highest coordination appears in $C2/c$ Li_6P (4 formula units), in which P atoms coordinate with 18 nearest-neighbor Li atoms (Figure 2e). These coordination numbers are much higher than the previously calculated highest 14-fold coordination in $P6/mmm$ Li_5P [36]. All Li-P phases are compactly assembled P-Li polyhedrons (a more detailed structural information can be found in the Supporting Information, Table S1).

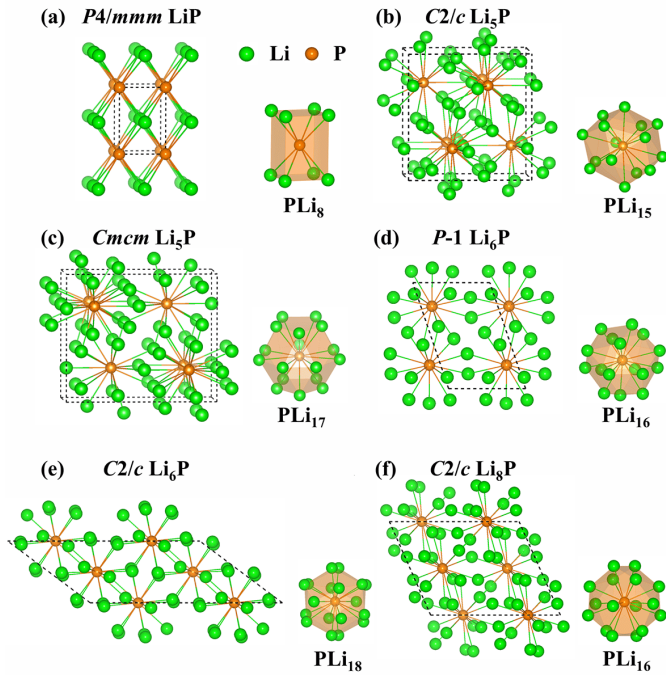


Figure 2. Structural features of stable Li-P phases at high pressures. (a) $P4/mmm$ LiP at 200 GPa. (b) $C2/c$ Li_5P at 200 GPa. (c) $Cmcm$ Li_5P at 300 GPa. (d) $P-1$ Li_6P at 200 GPa. (e) $C2/c$ Li_6P at 300 GPa. (f) $C2/c$ Li_8P at 200 GPa. In all these structures, green and orange spheres represent Li and P atoms, respectively.

Electronic properties of Li_xP

Although P atom is hypercoordinated in all these Li-rich phosphide phases, Bader charge analysis does not conclude it has a hypervalence in any of them (Table S2). After getting three electrons from Li atoms, P atoms in Li-rich Li_xP ($x \geq 3$) fill completely their electronic shells. As a result, the rest of electrons offered by Li atoms accommodate into the lattice spaces, which induce the formation of electrides (Figures S3 and S6). The electronic band structures show that these electrides are metallic at the PBE level ($P6/mmm$ Li_5P at 100 GPa, $C2/c$ Li_5P at 200 GPa, $Cmcm$ Li_5P at 300 GPa, $P-1$ Li_6P at 200 GPa, $C2/c$ Li_6P at 300 GPa and $C2/c$ Li_8P at 300GPa) (Figures S4 and 3c). Additionally, $P4/mmm$ LiP , without interstitial electrons, is also metallic with a dominant P 3p orbital contribution (Figure S5). In contrast, $Fm-3m$ Li_3P remains insulating until 300 GPa, as a result of a strong ionic bonding between Li and P, due to the high matching among 3Li^+ and P^{3-} ions, which goes against closing the band.

As difference charge density in Figure 3a clearly shows, excess electrons in the highest coordinated $C2/c$ Li_6P assemble into interstitials on the planes of phosphorus atoms, $(0\ 1/3\ 0)$, having the dumbbell-like electride states (Figure S6). More interestingly, these dumbbell-like electride states interconnect each other across intermediate extranuclear electrons of P atoms, which is in sharp contrast with pressure induced isolated electride states in alkaline and alkaline-earth metals with insulating character[8]. This feature is further supported by its electron localization function (ELF)[37] (Figure. S6). These connected electronic channels in $C2/c$ Li_6P favors the electronic conductivity, and the contribution of interstitial electrons to the metallic state is illustrated in the projected density of states (PDOS, Figure 3d). Although the main contribution at the Fermi level comes from Li 2p orbitals, it has an important contribution associated to the interstitial electrons. In contrast, as P atoms fill their electronic shells by attaining three electrons from Li atoms, P 3s and 3p orbitals barely reach the Fermi level. As shown in Figure S7, a well-defined Fermi surface nesting appears in Li_6P along Γ M (Figure 3b), with highly dispersive bands in this direction (Figure 3c). Conversely, flatter bands associated to more localized electronic states appear along Γ V and L A. As discussed above, nearly three electrons in $C2/c$ Li_6P reside in the interstitials. In order to

show this, we have built a hypothetical system by removing three electrons from $C2/c$ Li_6P , $[\text{Li}_6\text{P}]^{3+}$. The absence of interstitial electrons in both ELF and charge density difference of $[\text{Li}_6\text{P}]^{3+}$ (Figures S8a and S8b) confirm that these excess electrons are responsible for the electroneutral states.

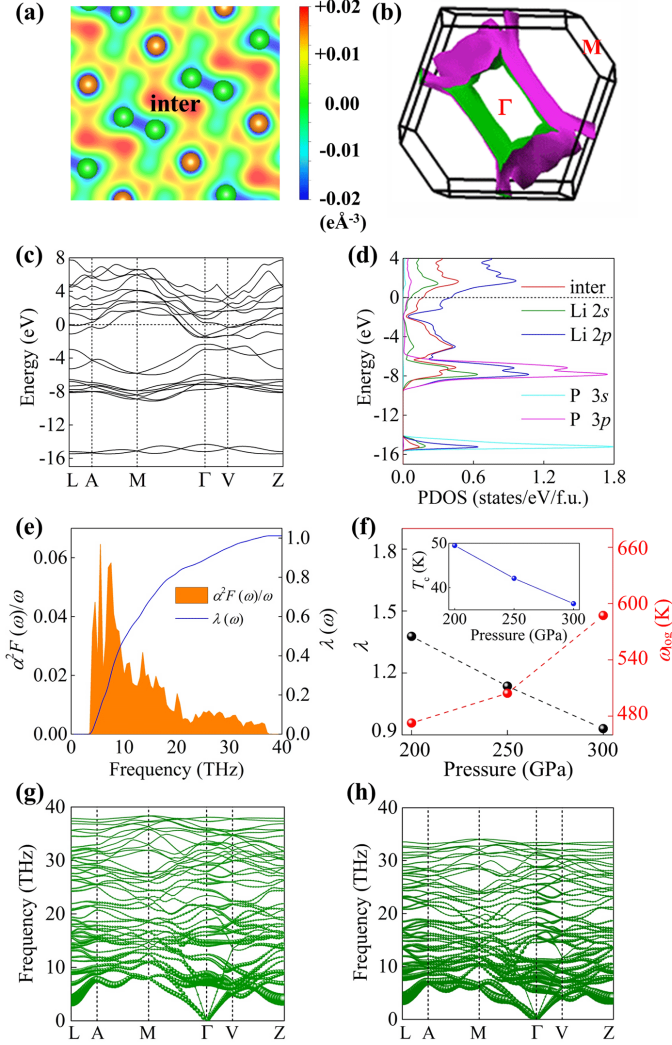


Figure 3. Electronic and superconducting properties of $C2/c$ Li_6P . (a) Difference charge density (crystal density minus superposition of isolated atomic densities) for $C2/c$ Li_6P plotted on the $(0 \ 1/3 \ 0)$ plane at 300 GPa. (b) The nested Fermi surface along the Γ M direction for $C2/c$ Li_6P . The Fermi surface of each band crossing the Fermi energy is shown in Figure S7. (c) The electronic band structure of $C2/c$ Li_6P at 300 GPa. (d) PDOS of $C2/c$ Li_6P at 300 GPa. The red line labeled by “inter” is obtained by projecting onto the interstitial orbitals (interstitial-site-centered spherical harmonics in empty spheres with a Wigner-Seitz radius of 1.0 Å). (e) Eliashberg spectral function (orange area) and frequency-dependent electron-phonon coupling

parameters $\lambda(\omega)$ (blue line) of $C2/c$ Li_6P at 270 GPa. (f) The electron-phonon coupling coefficient λ (black dashed line) and the logarithmic average phonon frequency ω_{\log} (red dashed line) as a function of pressure. The critical temperatures T_c (blue line) as a function of pressure is shown in the inset. The calculated phonon dispersion curves of $C2/c$ Li_6P at 300 (g), and 200 GPa (h). The area of each circle is proportional to the partial electron-phonon coupling, $\lambda_{q,v}$.

Superconductivity in Li_xP

Subsequently, we have calculated the superconducting T_c of all the metallic Li-P phases as estimated from the McMillan-Allen-Dynes formula[38-40]:

$$T_c = \frac{\omega_{\log}}{1.2k_B} \exp\left[-\frac{1.04(1+\lambda)}{\lambda - \mu^*(1+0.62\lambda)}\right]. \quad (2)$$

Here, k_B is the Boltzmann constant and μ^* is the Coulomb pseudopotential ($\mu^* = 0.1$). The electron-phonon coupling constant, λ , and the logarithmic average phonon frequency, ω_{\log} , are calculated by the Eliashberg spectral function for electron-phonon interaction:

$$\alpha^2 F(\omega) = \frac{1}{N(E_F)} \sum_{kq,v} |g_{k,k+q,v}|^2 \delta(\epsilon_k) \delta(\epsilon_{k+q}) \delta(\omega - \omega_{q,v}) \quad (3)$$

where $\lambda = 2 \int d\omega \frac{\alpha^2 F(\omega)}{\omega}$; $\omega_{\log} = \exp\left[\frac{2}{\lambda} \int \frac{d\omega}{\omega} \alpha^2 F(\omega) \ln(\omega)\right]$.

Herein, $N(E_F)$ is the electronic density of states at the Fermi level, $\omega_{q,v}$ is the phonon frequency of mode v and wave vector q , and $|g_{k,k+q,v}|$ is the electron-phonon matrix element between two electronic states with momenta k and $k+q$ at the Fermi level[41,42].

Table 1. Superconducting properties of the metallic Li-P phases.

Phases	Pressure (GPa)	λ	ω_{\log} (K)	$N(E_F)$ (states/Ry)	T_c (K)
$P4/mmm$ LiP	200	0.28	898.11	2.40	0.22
$C2/c$ Li_5P	200	0.40	634.89	7.41	2.61
$Cmcm$ Li_5P	300	0.25	683.50	4.43	0.05
$P-1$ Li_6P	200	0.41	619.35	8.07	2.87
$C2/c$ Li_6P	270	1.01	554.34	11.49	39.30
$C2/c$ Li_8P	200	0.50	575.54	10.14	7.15

Main superconducting characteristics are shown in Table 1. Although metallicity extensively exists in high-pressure Li-P compounds, most of them present a low T_c , except

$C2/c$ Li_6P , with a T_c of 39.30 K at 270 GPa. Actually, it is the highest T_c in an electride. The resulting electron-phonon coupling constant λ of $C2/c$ Li_6P is 1.01 at 270 GPa, which is comparable to the maximum value for Li_3S (1.43)[43] and H_2P (1.04)[44]. As can be seen in Figure 3e, low-frequency phonon modes dominate superconductivity, so that modes below 10 THz give a contribution of 52.4% to the electron-phonon coupling parameter λ at 270 GPa.

Although $C2/c$ Li_6P is metastable at pressures lower than 270 GPa, in order to better characterize the origin of its superconducting T_c , we have analyzed its evolution with pressure. As it is shown in Figure 3f, T_c increases as pressure reduces (36.4 K at 300 GPa; 49.49 K at 200 GPa), with a pressure coefficient (dT_c/dP) of -0.13 K/GPa. In addition, while λ decreases with pressure, ω_{log} increases. As it can be seen in Figure 3h, the contribution of low-frequency vibrations to the electron-phonon coupling is reduced with increasing of pressure. Interestingly, the softening along the Γ M direction decreases with pressure, which is correlated with the decreasing Fermi surface nesting. This nesting is associated with localized interstitial electrons, which are enhanced under lower pressure (Figure S9) and couple more strongly with phonons.

Conclusion

In this work we have analyzed pressure induced Li-rich phosphides under pressure up to 300 GPa. Although most of the electrides are non-metallic, in this work we report that pressure-induced stable Li_5P , Li_6P and Li_8P compounds are superconducting electrides. Among them, $C2/c$ Li_6P presents a T_c of 39.3 K at 270 GPa, which is the highest among the already known electrides. Superconductivity in these compounds can be attributed to a combination of a weak electronegativity of P with a strong electropositivity of Li. Excess electrons in the highest coordinated $C2/c$ Li_6P assemble into the interstitials on the planes of phosphorus atoms forming dumbbell-like anionic electrons, which play a dominant role in the superconducting transition. A Fermi surface nesting associated to localized electronic bands induces a phonon softening that enhances the electron-phonon coupling and favors the superconducting transition. These results open up the interest to explore high-temperature superconductivity in similar binary compounds.

Computational Method

To search the thermodynamically stable candidates of Li-P alloys under pressure, we have employed the swarm-intelligence based CALYPSO structure prediction method, which can efficiently find the stable structures just depending on the given chemical compositions[45,46]. The CALYPSO method has made great achievements in predicting new compounds[22,47-50]. Structural optimization and electronic property calculations were performed in the framework of density functional theory (DFT)[51,52] within the Perdew–Burke–Ernzerhof of the generalized gradient approximation (GGA)[53] as implemented in the VASP5.3 code[54]. The electron–ion interaction is described by pseudopotentials built within the scalar relativistic projector augmented wave (PAW)[55] method with $3s^23p^3$ valence electrons for P, and $1s^22s^12p^0$ valence electrons for Li. A cutoff energy of 500 eV and Monkhorst-Pack k -meshes[56] with a grid spacing of $2\pi \times 0.025 \text{ \AA}^{-1}$ were used to yield a good convergence for the enthalpy. To determine the dynamic stability of the predicted structures, phonon calculations were performed by using the finite displacement approach as implemented in the Phonopy code[57]. Superconducting properties were calculated based on density functional perturbation theory and the plane-wave pseudopotential method with Vanderbilt-type ultrasoft pseudopotentials, as implemented in the QUANTUM ESPRESSO code[58]. Detailed descriptions of structural predictions and computational details can be found in the Supporting Information.

Acknowledgements

This work is supported by the Natural Science Foundation of China under Nos. 21573037, 11704062, and 51732003; the Natural Science Foundation of Jilin Province (No. 20150101042JC); the Postdoctoral Science Foundation of China (under Grant No. 2013M541283); and the Fundamental Research Funds for the Central Universities (2412017QD006). A.B. acknowledges financial support from the Spanish Ministry of Economy and Competitiveness (FIS2016-76617-P) and the Department of Education, Universities and Research of the Basque Government and the University of the Basque Country (IT756-13).

References

- [1] J. L. Dye, *Science* **301**, 607 (2003).
- [2] C. Park, S. W. Kim, and M. Yoon, *Physical Review Letters* **120**, 026401 (2018).
- [3] M. S. Miao and R. Hoffmann, *Journal of the American Chemical Society* **137**, 3631 (2015).
- [4] M. S. Miao and R. Hoffmann, *Accounts of chemical research* **47**, 1311 (2014).
- [5] M.-s. Miao, X.-l. Wang, J. Brgoch, F. Spera, M. G. Jackson, G. Kresse, and H.-q. Lin, *Journal of the American Chemical Society* **137**, 14122 (2015).
- [6] C. J. Pickard and R. J. Needs, *Physical review letters* **102**, 146401 (2009).
- [7] M. Martinez-Canales, C. J. Pickard, and R. J. Needs, *Physical review letters* **108**, 045704 (2012).
- [8] Y. Ma, M. Eremets, A. R. Oganov, Y. Xie, I. Trojan, S. Medvedev, A. O. Lyakhov, M. Valle, and V. Prakapenka, *Nature* **458**, 182 (2009).
- [9] P. Li, G. Gao, Y. Wang, and Y. Ma, *The Journal of Physical Chemistry C* **114**, 21745 (2010).
- [10] Y. Lu, J. Li, T. Tada, Y. Toda, S. Ueda, T. Yokoyama, M. Kitano, and H. Hosono, *Journal of the American Chemical Society* **138**, 3970 (2016).
- [11] J. Park *et al.*, *Journal of the American Chemical Society* **139**, 615 (2017).
- [12] J. Wang, K. Hanzawa, H. Hiramatsu, J. Kim, N. Umezawa, K. Iwanaka, T. Tada, and H. Hosono, *Journal of the American Chemical Society* **139**, 15668 (2017).
- [13] Y. Tsuji, P. L. V. K. Dasari, S. F. Elatresh, R. Hoffmann, and N. W. Ashcroft, *Journal of the American Chemical Society* **138**, 14108 (2016).
- [14] Y. Zhang, W. Wu, Y. Wang, S. A. Yang, and Y. Ma, *Journal of the American Chemical Society* **139**, 13798 (2017).
- [15] Y. Zhang, B. Wang, Z. Xiao, Y. Lu, T. Kamiya, Y. Uwatoko, H. Kageyama, and H. Hosono, *npj Quantum Materials* **2**, 45 (2017).
- [16] E. W. Huang, C. B. Mendl, S. Liu, S. Johnston, H.-C. Jiang, B. Moritz, and T. P. Devereaux, *Science* **358**, 1161 (2017).
- [17] E. H. Neto *et al.*, *arXiv preprint arXiv:1804.09185* (2018).
- [18] Q. Si, R. Yu, and E. Abrahams, *Nature Reviews Materials* **1**, 16017 (2016).
- [19] H. Hosono, A. Yamamoto, H. Hiramatsu, and Y. Ma, *Materials Today* **21**, 278 (2017).
- [20] S. Qian, X. Sheng, X. Yan, Y. Chen, and B. Song, *Physical Review B* **96**, 094513 (2017).
- [21] D. Duan *et al.*, *Scientific Reports* **4**, 6968 (2014).
- [22] F. Peng, Y. Sun, C. J. Pickard, R. J. Needs, Q. Wu, and Y. Ma, *Physical Review Letters* **119**, 107001 (2017).
- [23] M. Miyakawa, S. W. Kim, M. Hirano, Y. Kohama, H. Kawaji, T. Atake, H. Ikegami, K. Kono, and H. Hosono, *Journal of the American Chemical Society* **129**, 7270 (2007).
- [24] T.-N. Ye, J. Li, M. Kitano, and H. Hosono, *Green Chemistry* **19**, 749 (2017).
- [25] Y. Kohama, S. W. Kim, T. Tojo, H. Kawaji, T. Atake, S. Matsuishi, and H. Hosono, *Physical Review B* **77**, 092505 (2008).
- [26] Y. Toda, Y. Kubota, M. Hirano, H. Hirayama, and H. Hosono, *ACS nano* **5**, 1907 (2011).
- [27] Y. Ge, S. Guan, and Y. Liu, *New Journal of Physics* **19**, 123020 (2017).
- [28] Y. Yao, S. T. John, and D. D. Klug, *Physical review letters* **102**, 115503 (2009).
- [29] C. L. Guillaume, E. Gregoryanz, O. Degtyareva, M. I. McMahon, M. Hanfland, S. Evans, M. Guthrie, S. V. Sinogeikin, and H. K. Mao, *Nature Physics* **7**, 211 (2011).
- [30] A. R. Oganov, Y. Ma, Y. Xu, I. Errea, A. Bergara, and A. O. Lyakhov, *Proceedings of the National Academy of Sciences* **107**, 7646 (2010).
- [31] M. Gatti, I. V. Tokatly, and A. Rubio, *Physical review letters* **104**, 216404 (2010).
- [32] M. Marqués, M. I. McMahon, E. Gregoryanz, M. Hanfland, C. L. Guillaume, C. J. Pickard, G. J. Ackland, and R. J. Nelmes, *Physical review letters* **106**, 095502 (2011).
- [33] X. Dong, Y.-L. Li, A. R. Oganov, K. Li, H. Zheng, and H.-k. Mao, *arXiv preprint arXiv:1603.02880* (2016).
- [34] R. Zhang, J. Waters, A. K. Geim, and I. V. Grigorieva, *Nature communications* **8**, 15036 (2017).
- [35] J. A. Flores-Livas, A. Sanna, A. P. Drozdov, L. Boeri, G. Profeta, M. Eremets, and S. Goedecker, *Physical Review Materials* **1**, 024802 (2017).
- [36] Z. Zhao, L. Liu, T. Yu, G. Yang, and A. Bergara, *The Journal of Physical Chemistry C* **121**, 21199 (2017).
- [37] A. D. Becke and K. E. Edgecombe, *The Journal of Chemical Physics* **92**, 5397 (1990).
- [38] L. N. Oliveira, E. K. U. Gross, and W. Kohn, *Physical review letters* **60**, 2430 (1988).
- [39] M. Lüders, M. A. L. Marques, N. N. Lathiotakis, A. Floris, G. Profeta, L. Fast, A. Continenza, S. Massidda, and E.

-
- K. U. Gross, *Physical Review B* **72**, 024545 (2005).
- [40] M. A. L. Marques, M. Lüders, N. N. Lathiotakis, G. Profeta, A. Floris, L. Fast, A. Continenza, E. K. U. Gross, and S. Massidda, *Physical Review B* **72**, 024546 (2005).
- [41] P. B. Allen and B. Mitrović, *Solid State Physics* **37**, 1 (1983).
- [42] J. P. Carbotte, *Reviews of Modern Physics* **62**, 1027 (1990).
- [43] C. Kokail, C. Heil, and L. Boeri, *Physical Review B* **94**, 060502 (2016).
- [44] A. Shamp, T. Terpstra, T. Bi, Z. Falls, P. Avery, and E. Zurek, *Journal of the American Chemical Society* **138**, 1884 (2016).
- [45] Y. Wang, J. Lv, L. Zhu, and Y. Ma, *Physical Review B* **82**, 094116 (2010).
- [46] Y. Wang, J. Lv, L. Zhu, and Y. Ma, *Computer Physics Communications* **183**, 2063 (2012).
- [47] J. Lv, Y. Wang, L. Zhu, and Y. Ma, *Physical review letters* **106**, 015503 (2011).
- [48] L. Zhu, H. Wang, Y. Wang, J. Lv, Y. Ma, Q. Cui, Y. Ma, and G. Zou, *Physical Review Letters* **106**, 145501 (2011).
- [49] H. Wang, S. T. John, K. Tanaka, T. Iitaka, and Y. Ma, *Proceedings of the National Academy of Sciences* **109**, 6463 (2012).
- [50] X. Wang, R. Xiao, H. Li, and L. Chen, *Physical Review Letters* **118**, 195901 (2017).
- [51] W. Kohn and L. J. Sham, *Physical Review* **140**, A1133 (1965).
- [52] P. Hohenberg and W. Kohn, *Physical Review* **136**, B864 (1964).
- [53] J. P. Perdew, K. Burke, and M. Ernzerhof, *Physical review letters* **77**, 3865 (1996).
- [54] G. Kresse and J. Furthmüller, *Physical review B* **54**, 11169 (1996).
- [55] P. E. Blöchl, *Physical review B* **50**, 17953 (1994).
- [56] J. D. Pack and H. J. Monkhorst, *Physical Review B* **16**, 1748 (1977).
- [57] A. Togo, F. Oba, and I. Tanaka, *Physical Review B* **78**, 134106 (2008).
- [58] P. Giannozzi *et al.*, *Journal of physics: Condensed matter* **21**, 395502 (2009).

Supporting Information

Superconductivity in Li₆P electrider

Ziyuan Zhao¹, Shoutao Zhang¹, Tong Yu¹, Haiyang Xu¹, Aitor Bergara^{*,2,3,4} and Guochun Yang^{*,1}

¹*Centre for Advanced Optoelectronic Functional Materials Research and Laboratory for UV Light-Emitting Materials and Technology of Ministry of Education, Northeast Normal University, Changchun 130024, China.*

²*Departamento de Física de la Materia Condensada, Universidad del País Vasco, UPV/EHU, 48080 Bilbao, Spain*

³*Donostia International Physics Center (DIPC), 20018 Donostia, Spain*

⁴*Centro de Física de Materiales (CFM), Centro Mixto CSIC-UPV/EHU, 20018 Donostia, Spain*

*Address correspondence to: a.bergara@ehu.eus; yanggc468@nenu.edu.cn.

Index	Page
1. Computational details	3
2. Convex hull of the Li-P system at 50 GPa.	5
3. Phonon dispersion curves of Li-P phases	6
4. The calculated electron localization function (ELF) for Li-P phases	6
5. The electronic band structures of Li-P phases	7
6. The projected density of states (PDOS) of <i>P4/mmm</i> LiP	7
7. ELF for <i>C2/c</i> Li ₆ P on the (0 1/3 0) plane	7
8. The Fermi surface of <i>C2/c</i> Li ₆ P at 300 GPa	8
9. ELF and difference charge density of [Li ₆ P] ³⁺	8
10. The ELF of interstitial electrons in Li ₆ P at 200 and 300 GPa	8
11. Bader charge analysis of P atoms in Li-rich phases	9
12. References	10

Computational Details

Our structural prediction approach is based on a global minimization of free energy surfaces merging *ab initio* total-energy calculations with CALYPSO (Crystal structure AnaLYsis by Particle Swarm Optimization) methodology as implemented in the CALYPSO code[1,2]. The structures of stoichiometry (Li_xP , $x = 1 - 8$) were searched with simulation cell sizes of 1-4 formula units (f.u.) at 50, 100, 200 and 300 GPa. In the first step, random structures with certain symmetry are constructed in which atomic coordinates are generated by the crystallographic symmetry operations. Local optimizations using the VASP code[3] were done with the conjugate gradients method and stopped when Gibbs free energy changes became smaller than 1×10^{-5} eV per cell. After processing the first generation structures, 60% of them with lower Gibbs free energies are selected to construct the next generation structures by PSO (Particle Swarm Optimization). 40% of the structures in the new generation are randomly generated. A structure fingerprinting technique of bond characterization matrix is applied to the generated structures, so that identical structures are strictly forbidden. These procedures significantly enhance the diversity of the structures, which is crucial for structural global search efficiency. In most cases, structural searching simulations for each calculation were stopped after generating 1000 ~ 1200 structures (e.g., about 20 ~ 30 generations).

To further analyze the structures with higher accuracy, we select a number of structures with lower enthalpies and perform structural optimization using density functional theory within the generalized gradient approximation[4] as implemented in the VASP code. The cut-off energy for the expansion of wavefunctions into plane waves is set to 500 eV in all calculations, and the Monkhorst–Pack k -mesh with a maximum spacing of $2\pi \times 0.025 \text{ \AA}^{-1}$ was individually adjusted in reciprocal space with respect to the size of each computational cell. This usually gives total energies well converged within ~ 1 meV/atom. The electron-ion interaction was described by using all-electron projector augmented-wave method (PAW) with $3s^23p^3$ valence electrons for P atom, $1s^22s^12p^0$ valence electrons for Li atom, respectively. To determine the dynamical stability of predicted structures, phonon calculations were performed by using the finite displacement approach as implemented in the Phonopy code.[5] In order to further test the reliability of the adopted pseudopotentials for Li and P, the validity of the projector augmented wave pseudopotentials from the VASP library is checked by comparing the calculated Birch-Murnaghan equation of state with that obtained from the full-potential linearized augmented plane-wave method (LAPW) using local orbitals (as implemented in WIEN2k[6]). The Birch-Murnaghan equation of states derived from PAW and LAPW methods are almost identical (Figure S0). Thus, our adopted pseudopotentials are feasible in the range of 50–300 GPa.

The electron-phonon coupling calculations are carried out with the density functional perturbation (linear response) theory as implemented in the QUANTUM ESPRESSO package.[7] We employ the ultrasoft pseudopotentials with $1s^22s^12p^0$ and $3s^23p^3$ as valence electrons for Li and P atoms, respectively. The kinetic energy cutoff for wave-function expansion is chosen as 40 Ry. To reliably calculate electron-phonon coupling in metallic systems, we need to sample dense k -meshes for electronic Brillouin zone integration and enough q -meshes for evaluating average contributions from the phonon modes. Dependent on specific structures of stable compounds, different k -meshes and q -meshes are used: $16 \times 16 \times 12$ k -meshes and $4 \times 4 \times 3$ q -meshes for LiP in the $P4/mmm$ structure, $12 \times 12 \times 6$ k -meshes and $4 \times 4 \times 3$ q -meshes for Li_5P in the $C2/c$ structure, $12 \times 12 \times 6$ k -meshes and $4 \times 4 \times 3$ q -meshes for Li_5P in the $Cmcm$ structure, $12 \times 12 \times 8$ k -meshes and $3 \times 3 \times 4$ q -meshes for Li_6P in the $P-1$ structure, $12 \times 12 \times 6$ k -meshes and $4 \times 4 \times 3$ q -meshes for Li_6P in the $C2/c$ structure, $15 \times 15 \times 8$ k -meshes and $3 \times 3 \times 4$ q -meshes for Li_8P in the $C2/c$ structure.

Supporting Figures

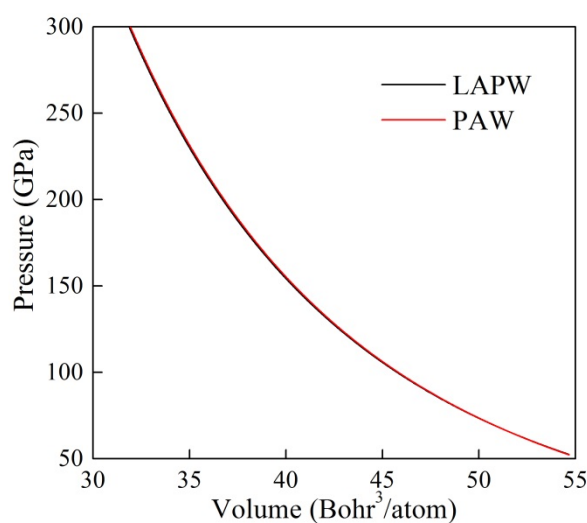


Figure S0. Comparison of the fitted Birch-Murnaghan equation of states for Li₅P with space group of *P6/mmm* by using the calculated results from the PAW pseudopotentials and the full-potential LAPW methods.

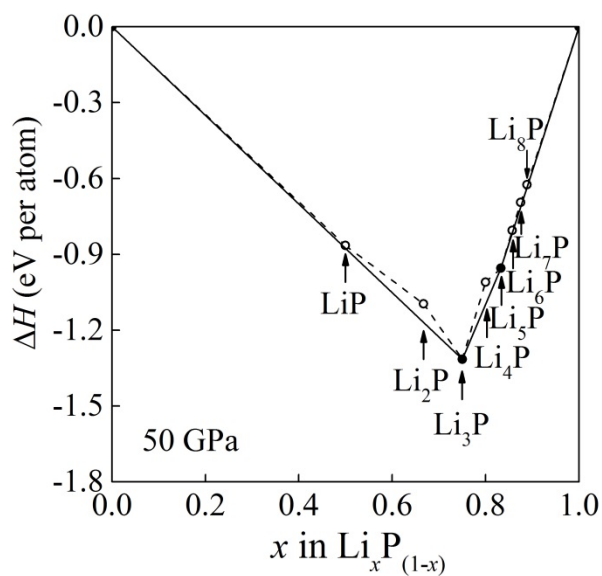


Figure S1. Relative thermodynamic stability of the Li_xP at 0 K and 50 GPa. The thermodynamically stable compounds are shown by solid symbols, connected by the convex hull line (solid lines).

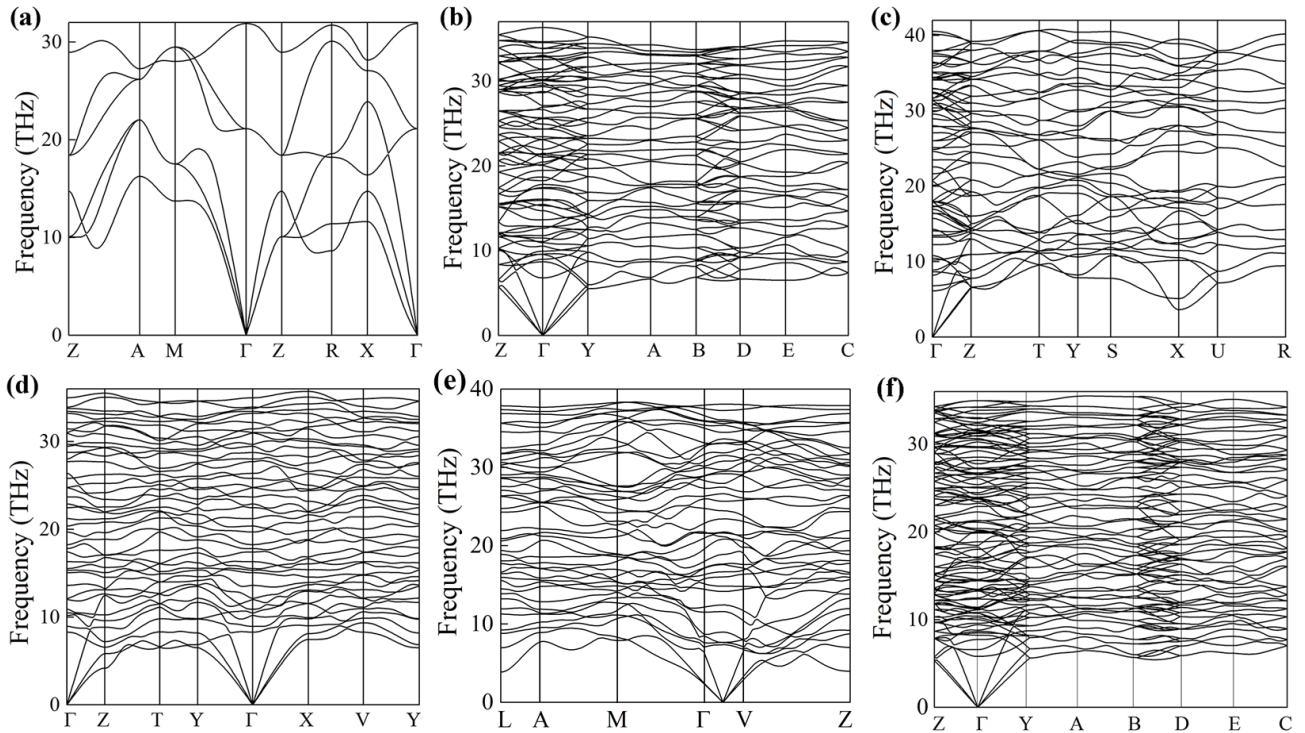


Figure S2. Phonon dispersion curves of metastable Li-rich phases. (a) $P4/mmm$ LiP at 200 GPa. (b) $C2/c$ Li₅P at 200 GPa. (c) $Cmcm$ Li₅P at 300 GPa. (d) $P-1$ Li₆P at 200 GPa. (e) $C2/c$ Li₆P at 300 GPa. (f) $C2/c$ Li₈P at 300 GPa. The absence of imaginary frequencies in these structures indicates they are dynamically stable.

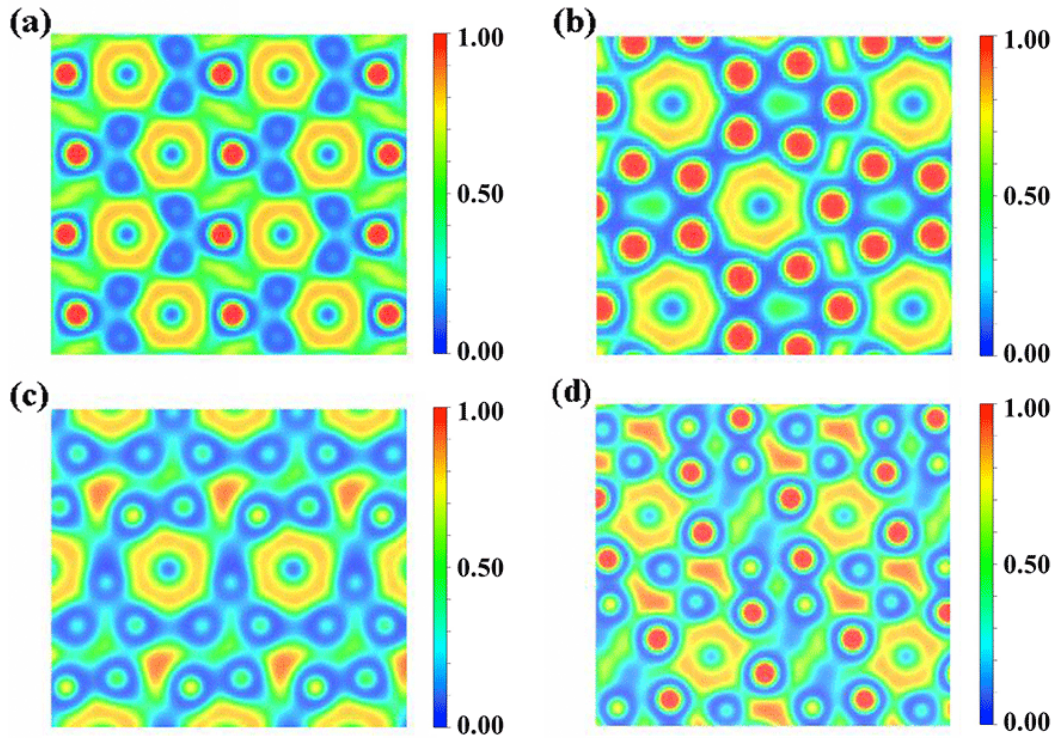


Figure S3. The calculated electron localization functions (ELF) for $C2/c$ Li₅P at 200 GPa (a), $Cmcm$ Li₅P at 300 GPa (b), $P-1$ Li₆P at 200 GPa (c), and $C2/c$ Li₈P at 300 GPa (d).

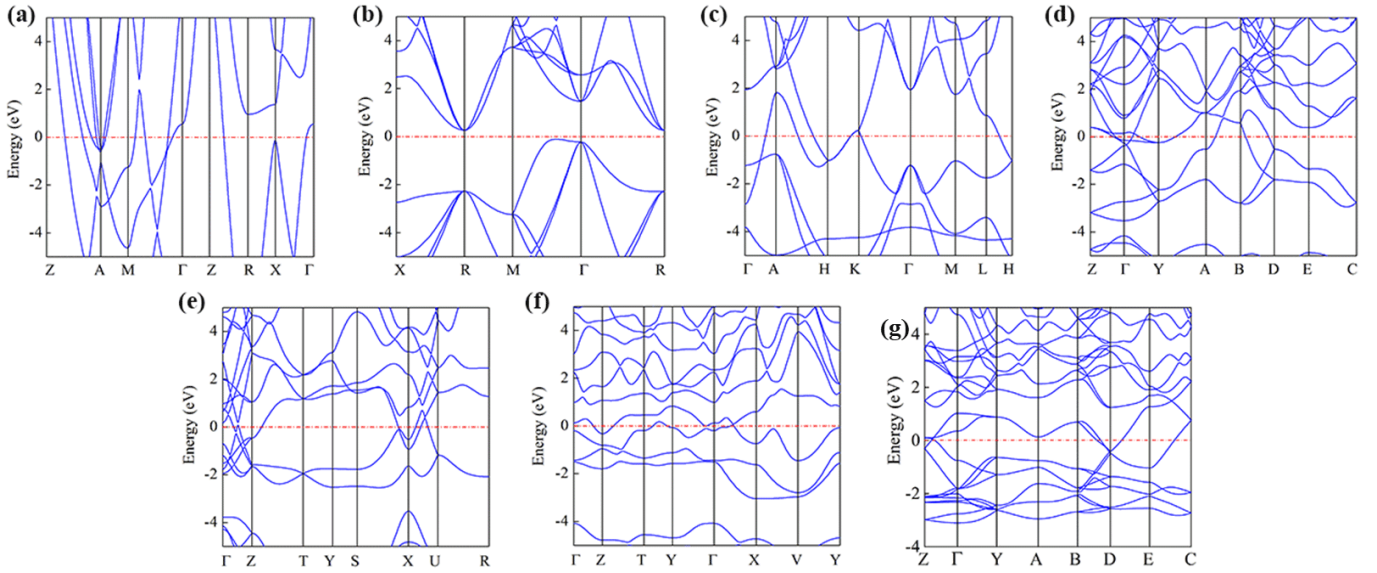


Figure S4. The electronic band structures have been calculated at the PBE level for $P4/mmm$ LiP at 300 GPa (a), $Fm-3m$ Li_3P at 300 GPa (b), $P6/mmm$ Li_5P at 100 GPa (c), $C2/c$ Li_5P at 200 GPa (d), $Cmcm$ Li_5P at 300 GPa (e), $P-1$ Li_6P at 200 GPa (f), and $C2/c$ Li_8P at 300 GPa (g). All the high symmetric paths in Brillouin zone are selected from unit cells.

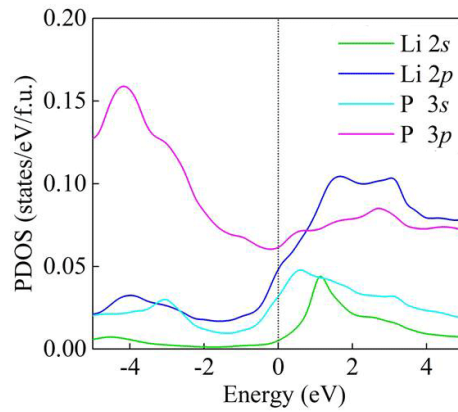


Figure S5. Projected density of states (PDOS) of $P4/mmm$ LiP at 300 GPa.

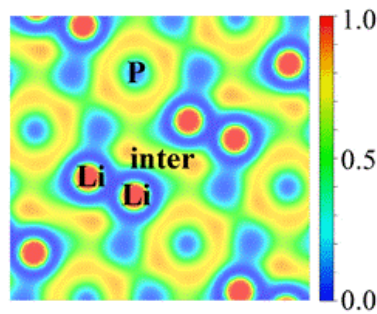


Figure S6. The calculated electron localization functions (ELF) for $C2/c$ Li_6P on the $(0 \ 1/3 \ 0)$ at 300 GPa. Electride states localize on the planes of phosphorus atoms, $(0 \ 1/3 \ 0)$ and $(0 \ 2/3 \ 0)$ planes, and their local features of the two mentioned planes are same. Therefore, only the calculated ELF on the $(0 \ 1/3 \ 0)$ is exhibited.

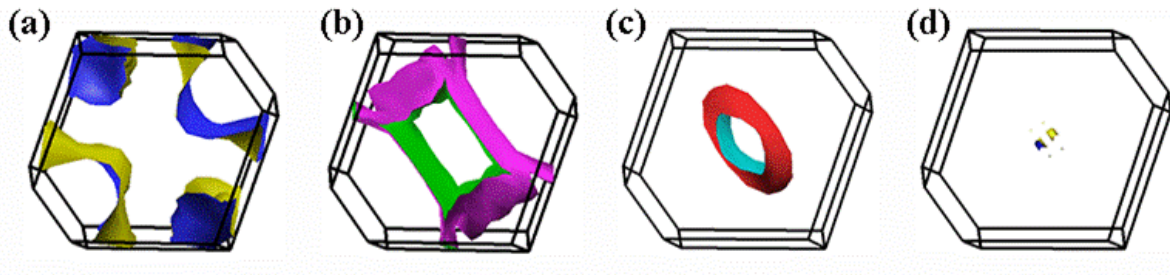


Figure S7. The Fermi surface associated to each band crossing the Fermi energy of $C2/c$ Li_6P at 300 GPa.

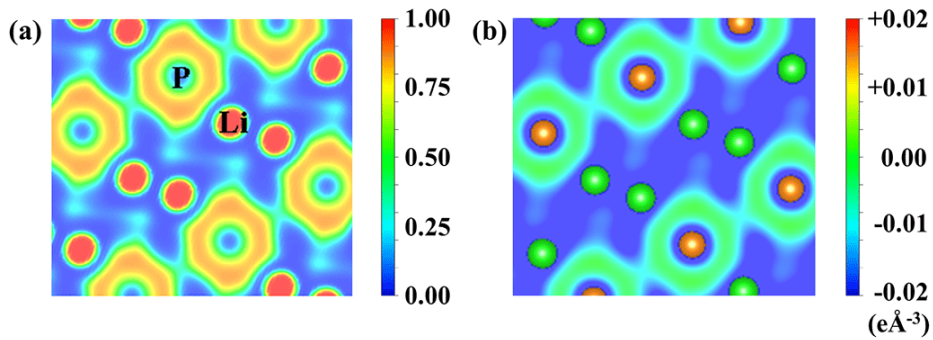


Figure S8. The ELF (a) and difference charge density (b) of $[\text{Li}_6\text{P}]^{3+}$ through removing 3 electrons per formula unit. The difference charge density of $C2/c$ $[\text{Li}_6\text{P}]^{3+}$ with removing 3 electrons is obtained by subtracting the charge density of the isolated Li and the isolated P atom from that of $C2/c$ Li_6P .

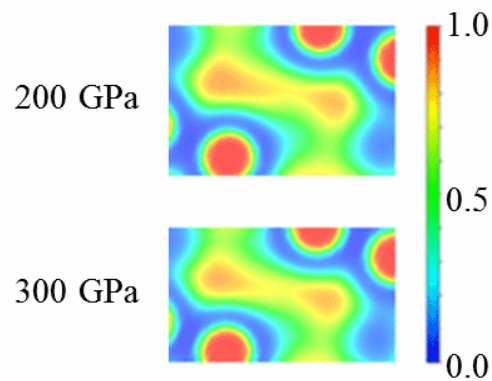


Figure S9. The ELF of interstitial electrons in $C2/c$ Li_6P at 200 and 300 GPa.

Supporting Tables

Table S2. Bader charge analysis of P atoms in Li-rich phases.

Phases	The number of electrons obtained from Li per P atom
<i>C2/c</i> Li ₅ P	2.88
<i>Cmcm</i> Li ₅ P	2.63
<i>P-1</i> Li ₆ P	2.93
<i>C2/c</i> Li ₆ P	3.00
<i>Imma</i> Li ₇ P	2.65
<i>C2/c</i> Li ₈ P	3.04

References

- [1] Y. Wang, J. Lv, L. Zhu, and Y. Ma, *Physical Review B* **82**, 094116 (2010).
- [2] Y. Wang, J. Lv, L. Zhu, and Y. Ma, *Computer Physics Communications* **183**, 2063 (2012).
- [3] G. Kresse and J. Furthmüller, *Phys. Rev. B* **54**, 11169 (1996).
- [4] J. P. Perdew, K. Burke, and M. Ernzerhof, *Physical review letters* **77**, 3865 (1996).
- [5] A. Togo, F. Oba, and I. Tanaka, *Physical Review B* **78**, 134106 (2008).
- [6] P. Blaha, K. Schwarz, P. Sorantin, and S. B. Trickey, *Computer Physics Communications* **59**, 399 (1990).
- [7] P. Giannozzi *et al.*, *Journal of physics: Condensed matter* **21**, 395502 (2009).